Enhanced Electrocatalysis of Oxygen Reduction on Pt/TaOx/GC

ARTICLE *in* THE JOURNAL OF PHYSICAL CHEMISTRY C · DECEMBER 2011

Impact Factor: 4.77 · DOI: 10.1021/jp209347r

5 AUTHORS, INCLUDING:

Zaenal Awaludin
Tokyo Institute of Technology
12 PUBLICATIONS **74** CITATIONS
SEE PROFILE

Jahangir Masud
Missouri University of Science and Technology
13 PUBLICATIONS **131** CITATIONS
SEE PROFILE

Takeo Ohsaka
Tokyo Institute of Technology
433 PUBLICATIONS **9,944** CITATIONS
SEE PROFILE

THE JOURNAL OF PHYSICAL CHEMISTRY C

ARTICLE

pubs.acs.org/JPCC

Enhanced Electrocatalysis of Oxygen Reduction on Pt/TaO_x/GC

Zaenal Awaludin, Masatoshi Suzuki, Jahangir Masud, Takeyoshi Okajima, and Takeo Ohsaka*

Department of Electronic Chemistry, Interdisciplinary Graduate School of Science and Engineering, Tokyo Institute of Technology, Mail Box G1-5, 4259 Nagatsuta, Midori-ku, Yokohama 226-8502, Japan

ABSTRACT: Here we demonstrate a remarkable enhancement of oxygen reduction reaction (ORR) activity on a novel Pt/TaO_x/GC electrocatalyst where at first tantalum oxide (TaO_x) and next Pt were deposited electrochemically on a glassy carbon (GC) surface. An excellent electrocatalytic activity of the Pt/TaO_x/GC electrocatalyst for ORR was found to be more than 12 times that of the unmodified Pt/GC one as evaluated from the kinetic currents at 0.80 V. SEM images showed no significant differences in the size and distribution of Pt nanoparticles between these two electrocatalysts, indicating that these are not factors causing the observed ORR activity. The spillover of oxygen-containing species resulting from the electronic interaction between Pt and TaO_x, which is evidently demonstrated from the XPS analysis, is strongly suggested as the crucial factor for the ORR enhancement. Interestingly, the spillover effect also results in a remarkable increase in the electrochemically active "apparent" surface area of Pt on the Pt/TaO_x/GC electrocatalyst. Moreover, the rotating ring-disk electrode voltammetric measurements obviously showed the increase in limiting current as well as the decrease in ring current on this novel electrocatalyst relative to the unmodified one, confirming a complete four-electron reduction pathway. On the basis of these findings a plausible mechanism has been proposed for the observed enhancement in ORR where the role of TaO_x is to reduce the formation of OH on the Pt surface by spillover effect and to promote d orbital vacancy of Pt for oxygen adsorption by electron donation to Ta.

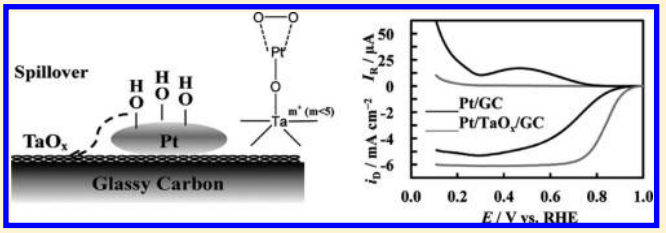

1. INTRODUCTION

A polymer electrolyte membrane fuel cell (PEMFC) is one of promising devices in energy conversion and greenhouse gas reduction.[1−4] This device converts chemical energy of fuel (H_2) directly into electrical energy, generally having a higher efficiency than conventional combustion engine.[1] However, the commercialization of PEMFC is predominantly hindered by a high content of Pt and slow kinetics of oxygen reduction reaction (ORR).[1,2,5−7] State-of-the-art Pt/C catalysts possess high activity of ORR at Pt loading of ca. 0.4 mg cm^{-2}, but lowering this Pt content causes a poor activity of the catalyst for ORR.[1,6] The agglomeration of Pt in the Pt/C catalyst[8−11] is also a serious problem to be resolved for achieving a highly active and durable catalyst for cathode in PEMFC.

The modification of Pt with transition metals (M) (M = Ni, Co, Fe, V, Ti) has resulted in a higher electrocatalytic activity toward ORR than pure Pt catalyst.[1−4,11−13] There have been several hypotheses to explain the enhancement of ORR on Pt-alloy catalysts. A lattice contraction of Pt−Pt bond distance is proposed to promote ORR by producing more sites for dissociative adsorption of oxygen.[14−16] An electronic interaction resulting in promoting the Pt-d band vacancy is also expected to play an important role for the enhancement of ORR on Pt alloys.[4,17] Meanwhile, other studies suggest that the increased ORR activity of Pt alloys is attributed to the inhibition of adsorbed OH (OH_{ad}) formation, which is confirmed from electrochemical and XANES data.[13,16] Practically, the use of Pt-alloys/C has resulted in a positive shift (ca. 20−40 mV) of the onset potential of ORR compared with Pt/C catalyst.[1,6] Therefore, this modification significantly increases the ORR activity of Pt, but the dissolution of the alloys is unhindered, particularly in acidic media.[18]

The effects of strong metal oxide-support interaction have attracted much attention in many catalytic reactions including ORR.[19−23] A spillover phenomenon, which was originally noticed and defined by Boudart et al.[24−26] for the heterogeneous catalysis of the Pt/WO_3 system is one of the effects introduced by this interaction that alter catalytic activity of noble metal.[21−29] The spillover of oxygen-containing species is also suggested as a main factor that enhances the electrocatalysis of ORR in the composites of Pt with metal oxide, MO_x (M = Mo, W, Ti).[23,30−37] The previous investigation by Bockris and McHardy predicted that the spillover of adsorbed species from platinum to Na_xWO_3 results in the increased velocity of the rate-determining species (RDS) of ORR on Pt surface and leads to the increase in reaction rate by 150 times compared with pure Pt catalyst.[34] Elezovic and coworkers[33] have also mentioned that the increase in catalytic activity of MoO_x−Pt/C, in comparison with Pt/C catalyst, could be explained through the increase in active sites for the ORR or by synergetic effects due to the formation of the interface between the platinum and oxide materials and by spillover due to surface diffusion of oxygen reaction intermediates. In addition, these metal oxide supports have a high stability in acidic environments and also help in preventing the supported Pt particles from aggregation.[8,38−42]

Received: September 27, 2011
Revised: November 6, 2011
Published: November 08, 2011

Tantalum and its oxides (TaO_x) have been regarded as very stable materials in acidic media due to the formation of a passive layer of Ta_2O_5.[41−45] TaO_x has also attracted much attention in many catalytic reactions such as esterification, alkylation, and oxidation of organic molecules.[46−48] To our knowledge, there have been only a few reports regarding the effect of TaO_x as insulator on ORR.[49,50] Baturina et al.[51] have reported that the Ta_2O_5/Pt/VC and Pt/Ta_2O_5/VC electrodes, in which the former was prepared by deposition of Pt colloids on Vulcan carbon (VC) and then Ta_2O_5, whereas the latter by the deposition of Ta_2O_5 on VC and then Pt colloids, give a decreased electrochemically active surface area (ECSA) resulting in a lower catalytic activity of ORR compared with the Pt-deposited VC electrode. A similar result was also reported by Bonakdarpour et al.[43] where the addition of Ta also caused a negative impact on the electrocatalytic activity of Pt toward ORR. Very recently, Wesselmark et al.[52] also reported that the Pt-deposited TaO_x electrode, in which TaO_x layer and then Pt layer were deposited on a gas diffusion layer (GDL) by thermal evaporation in vacuum, resulted in a significant loss of ECSA and ORR activity. In contrast with these reports, recently, our group[53] has demonstrated that amorphous TaO_x electrodeposited Pt (TaO_x/Pt) electrode, which was prepared by electrodeposition of TaO_x on Pt electrode in propylene carbonate (PC), possesses a remarkably enhanced catalytic activity toward ORR in acidic media. The onset potential of ORR at the TaO_x/Pt electrode positively shifted with a decrease in production percentage of hydrogen peroxide (H_2O_2) in comparison with that at the pure Pt. The different electrocatalysis of TaO_x composites for ORR, which largely depends on the procedures of their preparation, has not been essentially clarified yet.

In the present study, we have successfully developed a novel composite electrocatalyst of Pt nanoparticles-deposited TaO_x modified glassy carbon (Pt/TaO_x/GC) with a high electroactivity for ORR with a low Pt content. The Pt/TaO_x/GC electrocatalyst was prepared by the electrodeposition of TaO_x on GC substrate, followed by the electrodeposition of Pt nanoparticles. Cyclic voltammetry and rotating ring-disk electrode voltammetry were used to examine the electrochemical and electrocatalytic properties of this composite electrocatalyst, together with the surface characterization by scanning electron microscopy (SEM), X-ray diffraction (XRD) spectroscopy, and X-ray photoelectron spectroscopy (XPS). The so-called spillover phenomena of hydrogen and oxygen-containing species have been observed, demonstrating a remarkable increase in the real surface area of Pt. The XPS analysis on Pt and TaO_x suggested strong evidence of the metal oxide−support interaction. On the basis of the results obtained, a plausible mechanism has been proposed for the observed enhancement in ORR.

2. EXPERIMENTAL SECTION

The electrodeposition of TaO_x and Pt and electrochemical measurements was carried out in a standard three-compartment electrochemical cell using Pt spiral for counter electrode. All electrochemical experiments were conducted at room temperature (set at 25 °C) using an ALS/CH electrochemical analyzer (model 760 Ds). A reference electrode of Ag|AgCl|$KCl_{(sat)}$ was used where the cell was separated by a salt bridge from the reference compartment. Exceptionally, we used Ag wire as a reference electrode in the electrodeposition of TaO_x. All potentials are reported with respect to a reversible hydrogen electrode (RHE), unless otherwise noted.

2.1. Preparation of Electrocatalysts. Prior to the electrodeposition, a bare GC electrode (6 mm in diameter, 0.283 cm^2 of geometric surface area) was mechanically and electrochemically pretreated to produce a clean GC surface. First, a GC electrode was polished mechanically on emery paper with grid no. 2000. The polishing was followed with aqueous slurries of successively finer alumina powder (1 μm down to 0.06 μm) with the help of a polishing microcloth. To remove the slurries, the electrode was washed ultrasonically in >18 MΩ Millipore water for 10 min and electrochemically pretreated by polarizing the electrode at 2.0 V versus Ag|AgCl|$KCl_{(sat)}$ in Ar-saturated 0.1 M H_2SO_4 solution for 20 s to enhance the stability of Pt particles.[54,55]

The TaO_x was first electrodeposited on the pretreated GC electrode. The electrodeposition of TaO_x on the GC electrode was basically carried out according to our preceding report.[53] All chemicals were used as received either from Wako Pure Chemical Industries or Kanto Chemical without any further purification. PC solution containing 1 M lithium perchlorate ($LiClO_4$) and 0.05 M tantalum pentachloride ($TaCl_5$) were used as electrolyte and source of Ta, respectively. A cyclic potential scan technique was employed to deposit TaO_x on the GC in the potential range between 0.3 and −2.0 V versus Ag wire for two cycles at a scan rate of 20 mV s^{-1}. Just after the deposition of TaO_x, the electrode was soaked subsequently in methanol and water for 1 min to remove organic impurities on the GC surface. This electrode was then transferred to the electrochemical cell for the post-treatment, which was conducted by repeating the potential scan in the potential range between 0.06 and 1.46 V at a scan rate of 0.20 V s^{-1} for ca. 30 cycles or until a steady CV was obtained. The thus-prepared electrode will be hereinafter denoted as TaO_x/GC electrode. To complete the fabrication of Pt/TaO_x/GC electrocatalyst, we carried out the electrodeposition of Pt on the TaO_x/GC electrode in 0.1 M hydrochloric acid (HCl) solution containing 3 mM potassium hexachloroplatinate (K_2PtCl_6). A bipotential step technique was used to obtain nanosized particles of Pt according to the previous report.[56] First, the electrode was potentiostated at −1.24 V for 0.1 s, followed by the deposition of Pt at 0.02 V for 10 to 20 s. This method was expected to yield Pt particles with ca. 20 nm of size on the GC surface.[56] The amount of charge of Pt deposition was set so as to obtain ∼6 μg Pt cm^{-2}. After this deposition, the electrode was electrochemically pretreated by repeating the potential scan in the potential range between 0.06 and 1.30 V in Ar-saturated 0.1 M $HClO_4$ electrolyte solution at scan rate of 0.20 V s^{-1} for several cycles until a steady CV was obtained. The thus-prepared electrocatalyst will be hereinafter denoted as Pt/TaO_x/GC. The same technique of Pt electrodeposition was also applied to the bare GC substrate, and the prepared electrode will be denoted as Pt/GC electrocatalyst.

2.2. Surface Characterizations. In XPS measurements, the prepared electrocatalysts were placed under an ultra high vacuum (UHV) condition (1×10^{-6} Pa) where an ESCA-3400 electron spectrometer (SHIMADZU) with unmonochromatized X-ray source (Mg Kα ($h\nu$ = 1253.6 eV) anode, emission current: 20 mA, and acceleration voltage: 10 kV) was employed. For each measurement, all XPS spectra were corrected to the internal reference spectra of C 1s at 284.5 eV to compensate the electrostatic charging. Then, the core-level spectra were carefully deconvoluted to investigate the chemical states of elements on the electrocatalyst surface. For Ta $4f_{7/2}$ and $4f_{5/2}$ spectra, the binding energy gap and area ratio were kept constant at 1.9 and 1.4 eV, respectively.[57] For deconvolution of C 1s spectra, the

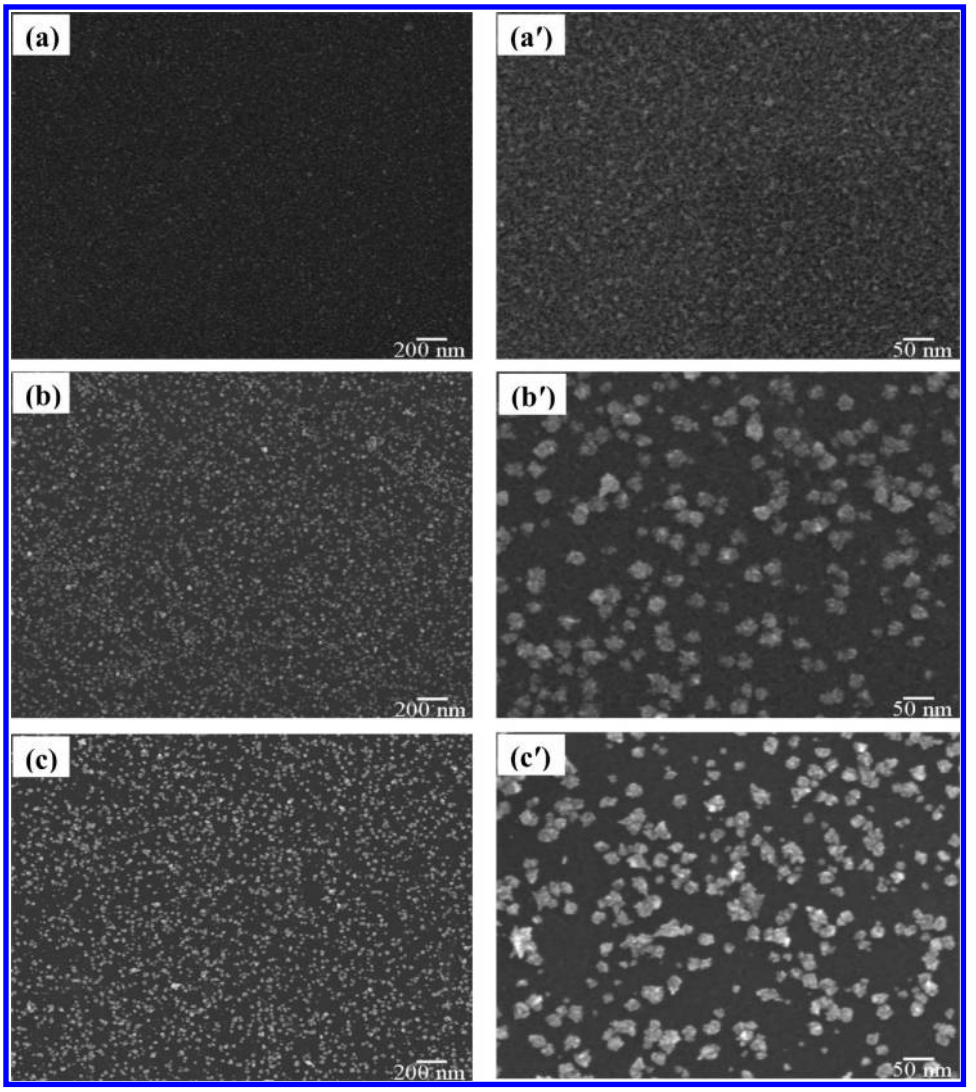

Figure 1. SEM images of TaO_x/GC (a,a′), Pt/TaO_x/GC (b,b′), Pt/GC (c,c′) electrocatalysts taken at two different magnifications.

value of full with at half-maximum (fwhm) was also fitted to 1.3 eV for sp^2 hybridization of C−C in pyrolytic graphite.[58] To take insight into the depth-profile of TaO_x, a pumped Ar^+ ion gun was sputtered to remove the oxide layer on the electrode surface. For SEM characterizations, the electrode surface was examined using an SEM S4700 (Hitachi). The XRD patterns were obtained from a diffractometer (Philips X′pert pro MRD), where the radiation source was obtained from Cu Kα. The measurements were performed from 30 to 90° and 35 to 50° at different scanning rates.

2.3. Electrochemical Measurements. The electrochemical characterizations were performed with the electrocatalyst immersed in 0.1 M $HClO_4$ solution where prior to each measurement the electrolyte solution was purged with either Ar or O_2 gas (99.999% of purity) for 25 min. In the ORR study, the RRDE voltammetric measurements were carried out using Nikko Keisoku Motor speed controller in O_2-saturated solution and recorded at various rotation rates. In this case, the Pt ring electrode was potentiostated at 1.2 V, where hydrogen peroxide was completely oxidized under a diffusion control. All current densities were normalized by the geometric surface area of electrode. The real Pt surface area of Pt/GC electrocatalyst, which is usually defined as ECSA, and the "apparent" Pt surface area of Pt/TaO_x/GC electrocatalyst were calculated by the conventional manner based on an electric charge for the hydrogen desorption,[59,60] supposing 210 μC cm^{-2} for a smooth polycrystalline Pt surface. In the case of the latter electrocatalyst, the thus-calculated Pt surface area reflects the so-called hydrogen spillover, as demonstrated in the present study and thus will hereinafter be denoted as "apparent" surface area.

3. RESULTS AND DISCUSSION

3.1. SEM, EDX, and XRD Analyses. The SEM images of TaO_x/GC, Pt/GC, and Pt/TaO_x/GC electrocatalysts were taken with different magnifications and are shown in Figure 1. In the case of the TaO_x/GC electrocatalyst (Figure 1a,a′), the TaO_x particles, estimated as about 1−3 nm in size, disperse homogenously on the GC surface. Figure 1b,b′,c,c′ shows a distribution of Pt particles on the Pt/TaO_x/GC and Pt/GC elctrocatalysts, respectively. As seen from these Figures, there is no marked difference in the distribution and morphology of Pt particles and TaO_x appears to have no significant effect on the Pt electrodeposition. However, interestingly, the Pt ion complex ($PtCl_6^{2-}$) was reduced at the TaO_x/GC electrode at more

dx.doi.org/10.1021/jp209347r |J. Phys. Chem. C 2011, 115, 25557–25567

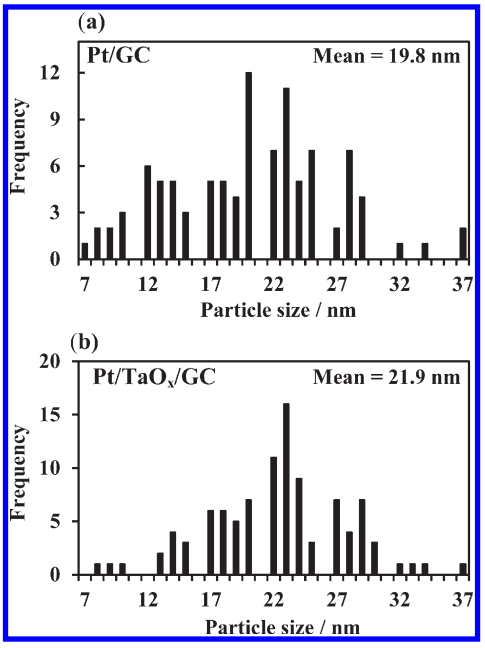

Figure 2. Histograms of size distribution of Pt particles in the Pt/GC (a) and Pt/TaO_x/GC (b) electrocatalysts obtained from random measurements of 100 particles (in Figure 1).

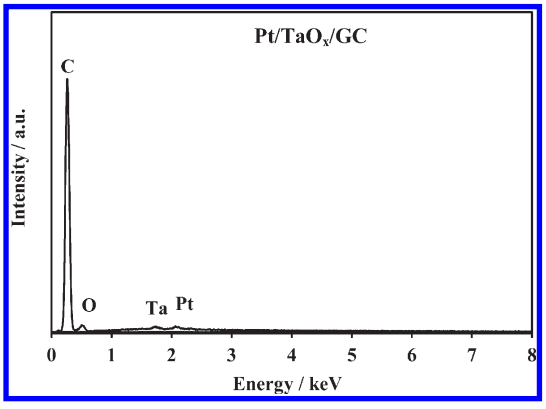

Figure 3. EDX spectrum of the surface of Pt/TaO_x/GC electrocatalyst.

positive potential compared with the bare GC electrode and for depositing the same amount of Pt, the time of electrolysis for the Pt deposition on the former electrode was shorter than that on the latter electrode. The detailed electrochemical behaviors will be reported elsewhere.

A distribution of Pt or Pt/TaO_x particle size on the Pt/GC and Pt/TaO_x/GC electrocatalysts is shown in Figure 2 in which 100 particles in the SEM images of both electrocatalysts were randomly selected and their size was measured. The mean sizes of particles are 19.8 and 21.9 nm for the Pt/GC and Pt/TaO_x/GC electrocatalysts, respectively. In addition, the particle size distribution of the Pt/TaO_x/GC electrocatalyst is narrower than that of the Pt/GC electrocatalyst. This may reflect the effect of TaO_x on the GC surface in the growth of Pt nuclei during the Pt deposition as anchor sites.[55]

The EDX pattern of the Pt/TaO_x/GC electrocatalyst (Figure 3) clearly shows an elemental characteristic of the surface, that is, the presence of C, O, and a small amount of Ta and Pt (extremely

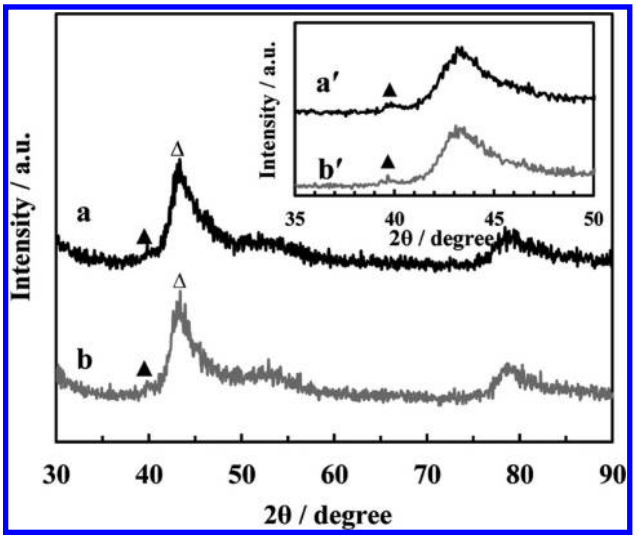

Figure 4. XRD patterns of the Pt/GC (a,a′) and Pt/TaO_x/GC (b,b′), electrocatalysts. The peaks indicated by Δ and ▲ correspond to the graphite (100) and Pt (111), respectively. The inset figure shows the XRD patterns of these electrocatalysts at a slower scan rate in the range of 2θ between 35 and 50°.

low intensities). A quantitative EDAX ZAF analysis revealed that the weight fractions of Ta and Pt are 0.88 and 0.61%, respectively. The XRD pattern shows the diffraction peak corresponding to the Pt (111) at 39.8°, but no diffraction peak corresponding to the Ta_2O_5 is observed (Figure 4).[53,61] The inset figure gives more apparent diffraction peaks, which were measured at lower scan rate. However, we could not observe any diffraction peak corresponding to Ta_2O_5 or TaO_x, which confirms an amorphous phase of TaO_x in the Pt/TaO_x/GC surface.

3.2. XPS Analysis. The electronic state of Ta after the electrodeposition on the GC surface was comprehensively studied by XPS, as shown in Figure 5. From the curve fitting after deconvolution (Figure 5a), it is clearly seen that Ta exists in one chemical state shown by a doublet peak at the binding energies of 26.4 and 28.3 eV corresponding to Ta $4f_{7/2}$ and Ta $4f_{5/2}$, respectively.[53,61,62] This means that these binding energies shift by 4.8 eV to the higher values with respect to the Ta metal; that is, the spectra correspond to the 5+ oxidation state of Ta, which is the most stable oxidation state of Ta.[57] The only oxidation state of 5+ of Ta as Ta_2O_5 was also observed in our previous studies.[53,62] To examine the oxidation states of Ta under the surface Ta_2O_5 layer, we performed a controlled erosion of the top layer of Ta_2O_5 via Ar^+—etching. The thus-obtained XPS spectrum is shown in Figure 5b. As demonstrated in this Figure, even after 1 min of Ar^+ etching, Ta^0 could not be observed: after deconvolution of the spectrum the lowest binding energy of Ta $4f_{7/2}$ was found to still be 2.9 eV higher than that of elemental Ta. So, we convincingly confirm that Ta metal does not exist in the deposit; that is, it is expressed as TaO_x ($0 < x \leq 5$). In addition, the observation of various peaks of TaO_x other than that corresponding to the Ta_2O_5 also suggests that Ta species of various oxidation states may contribute in the electrocatalytic activity of the Pt/TaO_x/GC for the ORR (mentioned below).

Figure 6 shows the typical XPS spectra of Pt 4f obtained at the Pt/TaO_x/GC and Pt/GC electrocatalysts in which the XPS spectrum for Pt plate is also given for comparison. The core-level spectra of Pt $4f_{7/2}$ and Pt $4f_{5/2}$ for the bulk Pt are 70.8 and

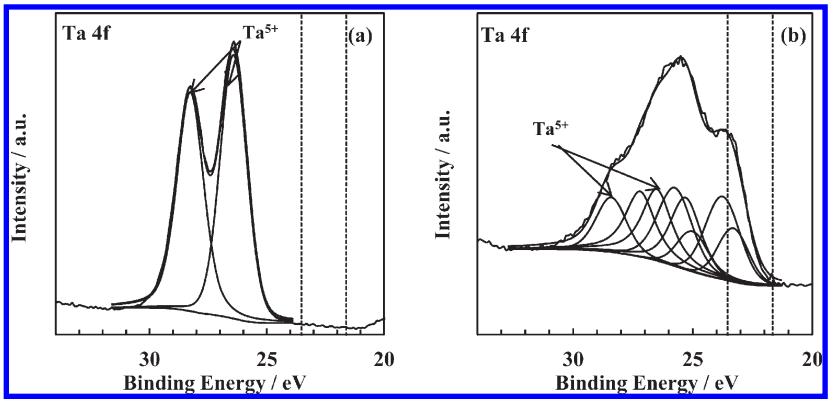

Figure 5. Ta (4f) XPS spectra of the TaO_x/GC electrocatalyst before (a) and after (b) Ar^+ etching for 1 min to observe the chemical states of Ta under the surface of Ta_2O_5 layer. The dotted lines correspond to the binding energies of $4f_{7/2}$ and $4f_{5/2}$ of elemental Ta.

74.1 eV, respectively. The fitted spectra of Pt $4f_{7/2}$ and Pt $4f_{5/2}$ for both Pt/TaO_x/GC and Pt/GC electrocatalysts shift to the higher binding energies (71.1 and 74.4 eV) with respect to those for the bulk Pt. This result strongly indicates an electronic interaction of Pt and the substrates.[55,63,64] In the case of the Pt/GC electrocatalyst, we suggested that the size effect of Pt particles could alter the binding energy of Pt 4f according to the explanation by Takasu and coworkers:[65] small particle size of Pt, that is, <4 nm, could result in the shift of Pt 4f core level spectra to the higher binding energy. However, in the present case, such a size effect cannot be expected because the size of Pt particles is in the range of ca. 7−37 nm with the mean size of ca. 20 nm (Figures 1 and 2). To track another possibility for the positive shift of Pt 4f core level spectra in the Pt/GC electrocatalyst, we attempted to deconvolute the spectra of C 1s, as displayed in Figure 7a. The peaks corresponding to the −OH, −CO, and −COO groups, which may be formed during the electrochemical pretreatment (oxidation) of the GC surface prior to the electrodeposition of Pt, were observed at 285.9, 288, and 288.9 eV, respectively. Interestingly, a broadening of C 1s spectra in the lower energy region was observed by the deconvolution. We found that the fitting error, $\Sigma\chi^2$, for the only one broad peak was larger than that for the deconvolution into two peaks by considering a possibly small peak in the lower binding energy region; finally, we obtained a small broad spectrum, which has a peak at 283.9 eV, that is, 0.6 eV lower than that of sp^2 bonding of graphitic carbon (284.5 eV), which suggests the electronic interaction between Pt and C (Pt−C).[55,63,64,66] This result is strongly supported by XPS C 1s spectra obtained at the Pt/TaO_x/GC electrocatalyst (Figure 7b), where the similar broad peak could not be observed, evidently meaning that in this case there is no Pt−C interaction, namely, Pt particles are deposited on the TaO_x layer but not on the GC surface. The Pt−C interaction resulting in the lower broadening of C 1s spectra has been previously reported for the thin Pt particles deposited on carbon-based materials.[55,64,66] Therefore, this Pt−C interaction may be suggested as the main cause of the positive shift of Pt 4f core level peaks in the Pt/GC electrocatalyst. This interaction was postulated originally by Hillendbrand and Lacksonen[63] as electron donation from Pt to the carbon support.

We also observed a positive shift (by 0.3 eV) of Pt 4f core level peaks at the Pt/TaO_x/GC electrocatalyst compared with those at the bulk Pt plate (Figure 6). To investigate this shift, we attempted to deconvolute carefully the Ta 4f spectra of the

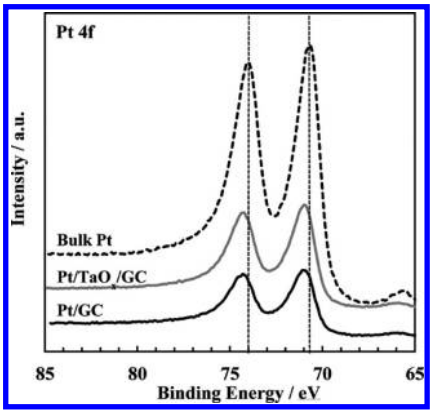

Figure 6. Pt (4f) XPS spectra of the Pt plate, Pt/TaO_x/GC and Pt/GC electrocatalysts. The Pt plate was used as reference to show a positive shift of Pt 4f binding energy at the Pt/TaO_x/GC and Pt/GC electrocatalysts. The dotted lines correspond to the binding energies of $4f_{7/2}$ and $4f_{5/2}$ of elemental Pt.

Pt/TaO_x/GC electrocatalyst. The value of $\Sigma\chi^2$ for only one pair of Ta$4f_{7/2}$ and $4f_{5/2}$ was found to be considerably larger than that for the deconvolution into two doublet spectra due to the broadening of the spectra at the lower binding energy. That is, in addition to a couple of Ta $4f_{7/2}$ and $4f_{5/2}$ corresponding to Ta^{5+}, we obtained that attributed to the oxidation state of <5+ for Ta (Figure 7c). This result may be explained by considering the following two possibilities. First, during the electrodeposition of Pt on the TaO_x/GC surface the potential was kept shortly at −1.24 V for 0.1 s, which might be sufficient to reduce Ta^{5+} in Ta_2O_5 into the lower state of oxidation number, that is, <5+. The second possibility is that the XPS spectra corresponding to Ta^{m+} (m < 5) could be the evidence of an electronic interaction between Pt and TaO_x. It is should be noted that we performed an electrochemical oxidation pretreatment for the Pt/TaO_x/GC electrode after the Pt deposition where the potential was scanned up to 1.30 V, which could oxidize the reduced TaO_x to regenerate Ta_2O_5 layer.[49] Moreover it is also well-established that Ta_2O_5 is chemically stable and the lower oxidation state is easily oxidized in an air atmosphere. Therefore, the second possibility is considered to be more reasonable for explaining the positive shift of Pt 4f spectra (Figure 6). In the case of the Ir−Al_2O_3 catalyst, Escard et al.[67] postulated an electron donation from Ir to the support of Al_2O_3. The electronic interaction between Pt and

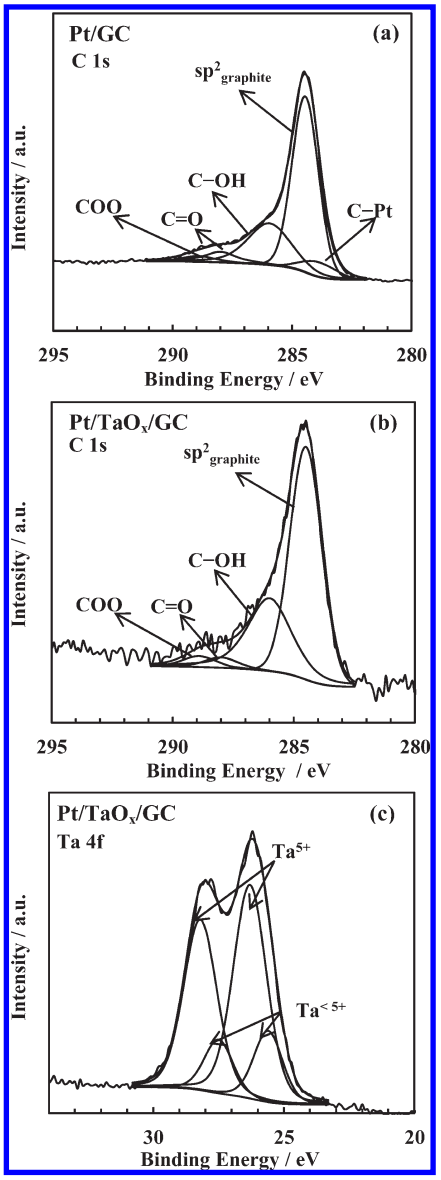

Figure 7. (a,b) C 1s and (c) Ta 4f spectra of the Pt/GC (a) and Pt/TaO_x/GC (b,c) electrocatalysts.

metal oxide support of TiO_2 was also modeled by Horsley,[68] who suggested a possibility of a strong interaction between Pt−O atoms. Further supporting evidence of metal oxide-support interaction was also reported by Chen et al.[46,47] for supported TaO_x catalysts on various metal oxides, and they demonstrated a significant influence of the oxide support through the bridging Ta−O−support bond on the catalytic activity for methanol oxidation. Therefore, on the basis of the present results, we can also propose the electronic interaction between Pt and TaO_x via the bridging by O atoms which forms a Ta−O−Pt bond.

3.3. CV and RRDE Voltammetry. Figure 8 shows cyclic voltammograms (CVs) obtained at the Pt/GC and Pt/TaO_x/GC electrocatalysts in Ar-saturated 0.1 M $HClO_4$ electrolyte solution. A characteristic CV response expected for Pt electrode is obtained for both the Pt/GC and Pt/TaO_x/GC electrocatalysts with a remarkable difference in the intensity of peak currents corresponding to the hydrogen adsorption−desorption and the oxide layer formation and its reduction. It should be noted here

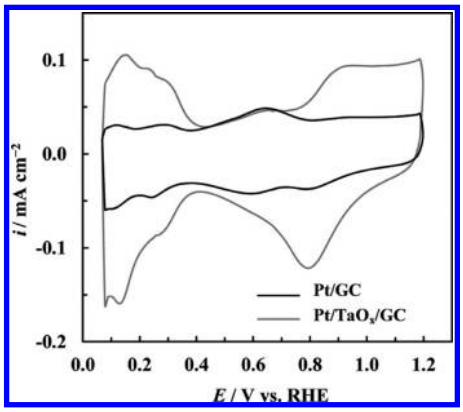

Figure 8. CVs obtained at the Pt/GC and Pt/TaO_x/GC electrocatalysts in Ar-saturated 0.1 M $HClO_4$ solution at scan rate of 50 mV s^{-1}.

that the amounts of Pt deposited on both electrocatalysts are the same (~6 μg cm^{-2}), but the "apparent" surface area of the Pt/TaO_xGC electrocatalyst is extremely larger than that of the ECSA of the Pt/GC electrocatalyst. The similar result was also observed by us for the TaO_x/Pt electrode in which TaO_x was electrodeposited on the Pt bulk electrode in the same way as that used in this study.[53] We strongly believe that the largely increased CV response observed for the Pt/TaO_x/GC electrocatalyst is related to the so-called spillover effect, where adsorbed H- and O-containing species are spilled over to and back-spilled over from the TaO_x, resulting from a strong metal oxide-support interaction between Pt and TaO_x, as also demonstrated for TiO_2−Pt and WO_3−Pt electrocatalysts.[22,27,31,35] Moreover, we also found that the characteristics of the Pt/TaO_x/GC electrocatalyst were also greatly affected by heat treatment, for example., the calcination at 600 °C under vacuum condition. This treatment could totally change the CV characteristics of the Pt/TaO_x/GC electrocatalyst where the spillover could not be observed and the characteristic peaks of Pt, corresponding to the hydrogen adsorption−desorption and oxide layer formation and its reduction, was markedly small at the calcinated one compared with the Pt/GC electrocatalyst. Then, we consider that a heat treatment might transform the molecular structure of TaO_x, causing an impairment of the electrochemical characteristics. A further study needs to be conducted to clarify such heat treatment effect. For this reason, here we consider only the as-prepared electrocatalysts.

An RRDE voltammetric technique is extremely useful in evaluating the catalytic activity of electrocatalyst for ORR as well as in clarifying ORR mechanism. Figure 9a shows the RRDE voltammograms for the ORR obtained at the Pt/GC- or Pt/TaO_x/GC-modified disk and Pt ring electrodes at rotation speed of 1600 rpm in O_2-saturated 0.1 M $HClO_4$ electrolyte solution. At first glance, we can see that the electrocatalysis of the Pt/TaO_x/GC electrocatalyst for the ORR is remarkably high compared with that of the Pt/GC one; the half-wave potential is shifted to the positive direction of potential, the disk current is increased, and the ring current is decreased. Moreover, although the loading amount of Pt is very small (~6 μg cm^{-2}) and the electrode surface of both electrocatalysts is not fully covered by Pt particles (Figure 1), the limiting current at the Pt/TaO_x/GC disk electrode is markedly high compared with that at the Pt/GC one, implying a complete four-electron pathway of ORR with the presence of TaO_x. Savadogo et al.[69] found that the increased

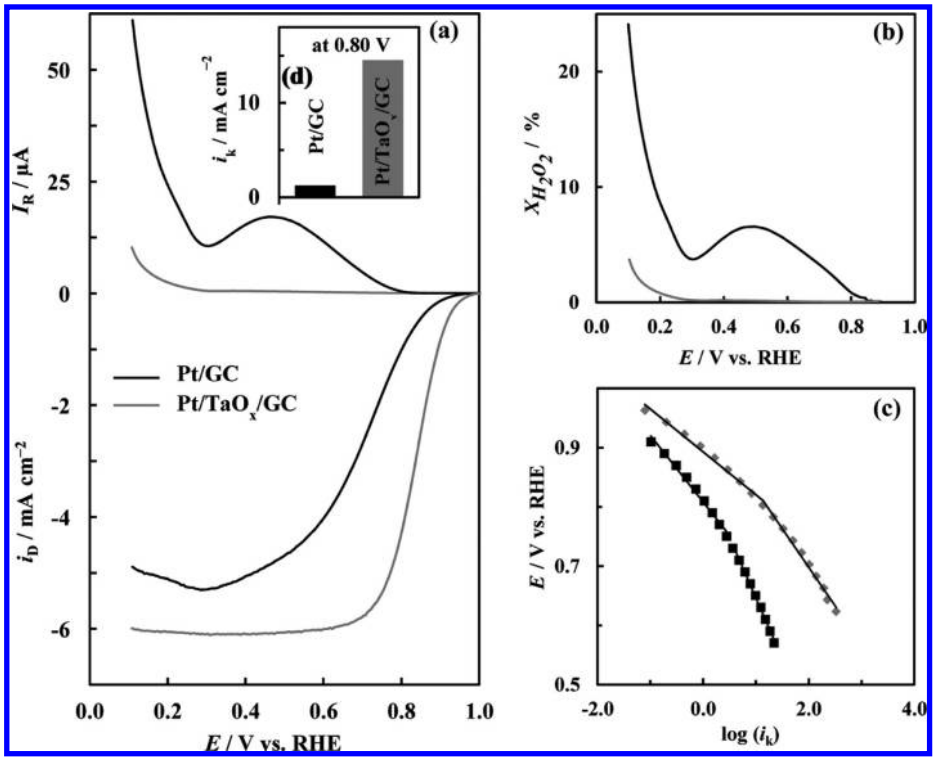

Figure 9. (a) Hydrodynamic voltammograms obtained at Pt/GC and Pt/TaO$_x$/GC modified-disk (i_D) and Pt ring (I_R) electrodes in O_2-saturated 0.1 M $HClO_4$ solution at scan rate of 5 mV s^{-1} (anodic scan) and rotation rate of 1600 rpm. The Pt ring electrode was potentiostated at 1.2 V. (b) Fraction of the hydrogen peroxide produced at the disk electrodes (calculated using eq 1). (c) Tafel plots where the i_k was obtained using eq 2. (d) Comparison of the i_k values at 0.80 V for Pt/GC and Pt/TaO$_x$/GC electrocatalysts.

Table 1. Electrochemical and Kinetics Parameters Obtained at Pt/GC and Pt/TaO$_x$/GC Electrocatalysts

electrode	ECSA or "apparent" surface area/m^2 g_{Pt}^{-1}	$E_{1/2}$/V	i_k/mA cm^{-2} at 0.85 V	i_k/mA cm^{-2} at 0.80 V	Tafel slope (lcd/hcd) /mV dec^{-1}
Pt/GC	7.6	0.70	0.48	1.2	−112/−205
Pt/TaO$_x$/GC	31.7	0.80	4.23	14.5	−72/−130

performance of the Pt-WO$_x$/C electrode for the ORR in H_3PO_4 at 180 °C compared with the Pt/C electrode is due to an increase in real surface area, although the cause for the increased surface area is not mentioned. Shim et al. found the improvement of the ORR performance and the increase in real surface are of Pt-WO_3/C and Pt-TiO_2/C electrocatalysts compared with the Pt/C electrocatalyst and explained that these are caused by synergistic effects that are based on adlineation due to formation of an interface between the platinum and oxide materials and by spillover due to surface diffusion of oxygen reaction intermediates.[35] On the basis of the same ideas, Elezovic et al. also explained the increase in catalytic activity for the ORR on MoO$_x$-Pt/C and TiO$_x$-Pt/C catalysts, in comparison with Pt/C catalyst.[32,33] As can be seen from Figure 8 and Table 1, the "apparent" surface area of the Pt/TaO$_x$/GC electrocatalyst is significantly larger than the ECSA of the Pt/GC electrocatalyst (4.2 times). Moreover, a largely decreased ring current was also observed at the Pt/TaO$_x$/GC electrode (i.e., it is close to zero in the potential range of 0.3 to 1.0 V) (Figure 9) as in the case of the ORR at the TaO$_x$/Pt electrode;[53] namely, a complete four-electron reduction of oxygen takes place at more positive potential than a potential (ca. 0.3 V) at which the hydrogen adsorption on the Pt surface starts. In contrast, a clear H_2O_2 oxidation current was observed at the Pt/GC electrocatalyst, strongly indicating that this electrocatalyst is much less active for the ORR due to a low ECSA value (7.6 m^2 g_{Pt}^{-1}).[60]

The percentage ($X_{H_2O_2}$/%) of H_2O_2 formed from one oxygen molecule at the disk electrode was calculated quantitatively using eq 1[70]

$$X_{H_2O_2} = \frac{2I_R N}{I_D + I_R/N} \times 100 \quad (1)$$

where N is the collection efficiency (0.372) and I_R and I_D are currents at the ring and disk electrodes, respectively. As can be seen from Figure 9b, $X_{H_2O_2}$ at the Pt/TaO$_x$/GC electrocatalyst is considerably small compared with that at the Pt/GC electrocatalyst; for example, at 0.1 V $X_{H_2O_2}$ is 24.1% at the Pt/GC electrocatalyst, whereas $X_{H_2O_2}$ is only 3.7% at the Pt/TaO$_x$/GC electrocatalyst and $X_{H_2O_2}$ is actually zero in the potential range of ca. 0.3 to 1.0 V. In the case of Pt alloys, a significant decrease in H_2O_2 production could not be observed.[12,13] The reduced H_2O_2 formation in the ORR was also demonstrated by Trogadas et al.[39] for the MnO_2/Pt/C and WO_3/Pt/C electrocatalysts in comparison with the unmodified Pt/C electrocatalyst.

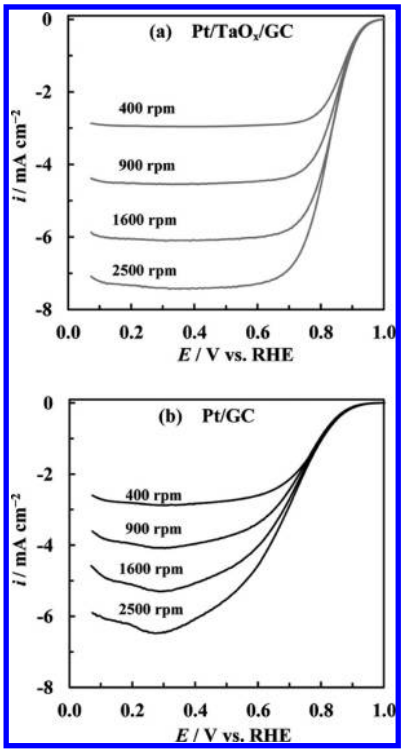

Figure 10. Hydrodynamic voltammograms obtained at the disk electrodes coated with (a) Pt/TaO$_x$/GC and (b) Pt/GC electrocatalysts in O_2-saturated 0.1 M $HClO_4$ solution at scan rate of 5 mV s^{-1} at various rotation rates.

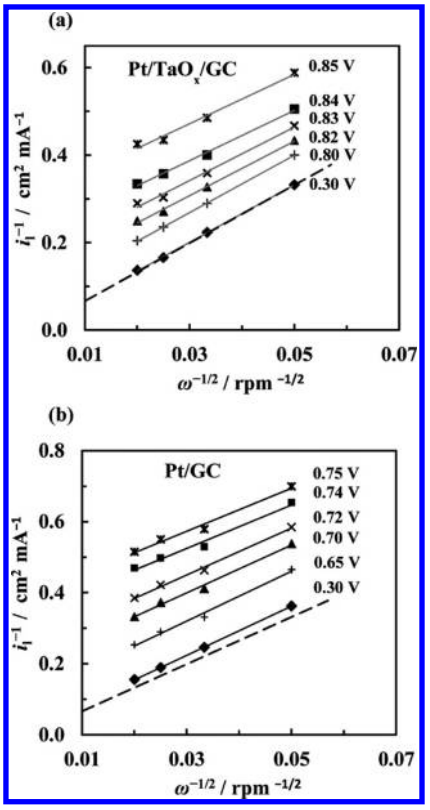

Figure 11. Koutecký−Levich plots at various potentials obtained at (a) the Pt/TaO$_x$/GC and (b) Pt/GC electrocatalysts (in Figure 10). The dashed line corresponds to the slope calculated for 4e$^-$ reduction pathway of ORR in O_2-saturated 0.1 M $HClO_4$ solution.

Figure 9c shows the mass-transfer corrected Tafel plots in which the kinetic current density (i_k) was obtained using Koutecký−Levich equation (eq 2)

$$\frac{1}{i_l} = \frac{1}{i_k} + \frac{1}{i_L} \tag{2}$$

where i_L and i_l are the mass-transfer limited current and the measured limiting current, respectively. As given in Figure 9c, the Pt/GC and Pt/TaO$_x$/GC electrocatalysts exhibit the typical Tafel plots with two slopes, at low and high current densities (lcd and hcd), as usually referred for both polycrystalline and nanosized Pt in aqueous solution.[12,13,71,72] The Tafel slopes obtained are given in Table 1 along with the other kinetic and electrochemical parameters of the ORR. It has been in general accepted that the two slopes at lcd and hcd regions are due to the change of adsorption of reaction intermediates from Temkin to Langmurian conditions or due to a change in the surface coverage by OH, which influences the adsorption of O_2 molecules.[70−72] As shown in Table 1, the slopes at lcd and hcd regions at the Pt/TaO$_x$/GC electrocatalyst are −72 and −130 mV dec^{-1}, respectively, which are much lower than those at the Pt/GC electrocatalyst (−112 and −205 mV dec^{-1} at lcd and hcd regions, respectively), implying that the ORR is faster at the Pt/TaO$_x$/GC than at the Pt/GC, as in the case of the Pt alloy catalysts.[12,13] At lower overpotential, the blocking of reaction sites for the ORR by adsorption of OH and O results in the deviation of the Tafel slope from its value at higher overpotential.[71−73] Therefore, the introduction of TaO$_x$ leads to the lowering of the Tafel slope and the positive shift (by 100 mV) of half-wave potential (Table 1). For the enhanced ORR at platinum-containing sodium tungsten bronze (Pt−Na$_x$WO$_3$), Bockris and McHardy suggested a model in which "spillover" of adsorbed intermediates from platinum to the bronze gives rise to an enhanced rate of oxygen reduction on the platinum.[34] Shim and coworkers[35] suggested that, based on the dependences of hydrogen desorption potential and oxide reduction potential upon the oxide content, metal oxide (e.g., WO_3 and TiO_2) near platinum can weaken the strength of the adsorption of hydrogen and oxygen on the surface of platinum; consequently, the ORR is enhanced. In the present case, we also expect that OH adsorbed on the Pt surface is spilled over to the TaO$_x$, which facilitates the first step of the ORR, that is, O_2 adsorption.

Figure 10 illustrates hydrodynamic voltammograms obtained for the ORR at the Pt/TaO$_x$/GC and Pt/GC electrocatalysts at different rotation rates. At a glance, it is obvious from the comparison of the voltammograms obtained at both electrocatalysts that the electrocatalysis of the Pt/TaO$_x$/GC electrocatalyst is much higher than that of the Pt/GC one. The transferred electron number per oxygen molecule involved in the ORR at the Pt/TaO$_x$/GC and Pt/GC electrocatalysts was determined by the Koutecký−Levich equation (eq 2) in which i_L is the Levich current and is expressed by eq 3

$$i_L = 0.62nFAD_{O_2}^{2/3}\nu^{-1/6}C_{O_2}\omega^{1/2} \tag{3}$$

where n is number of electrons transferred for per oxygen molecule, F is the Faraday constant (96 485 C mol^{-1}), A is geometric area of electrode (0.283 cm^2), D_{O_2} is the diffusion coefficient of O_2 (1.93×10^{-5} cm^2 s^{-1}),[13] ν is the kinetic viscosity of the solution (1.009×10^{-2} cm^2 s^{-1}),[13] and C_{O_2} is the

dx.doi.org/10.1021/jp209347r |J. Phys. Chem. C 2011, 115, 25557–25567

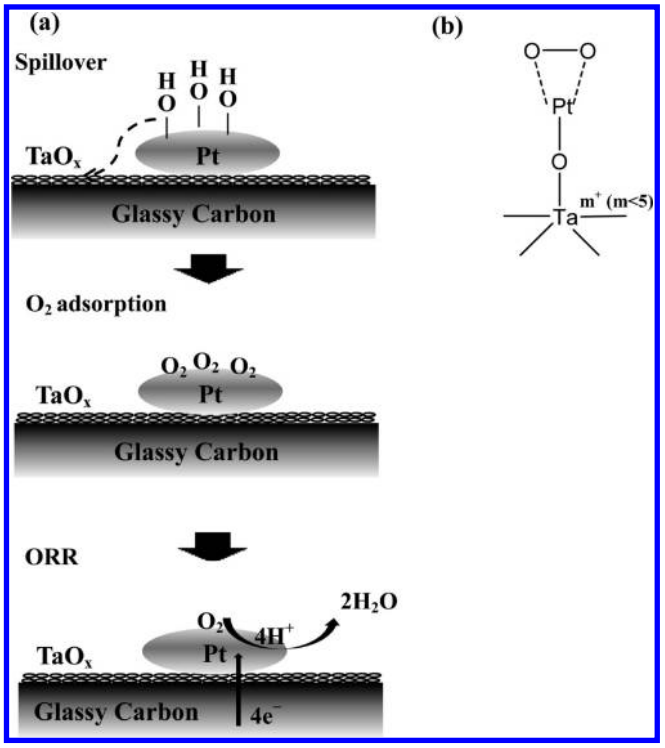

Figure 12. Schematic illustrations of (a) spillover effect of oxygen-containing species, that is, OH from Pt surface into TaO_x matrix in ORR, and (b) enhanced interaction of O_2 with Pt due to electron donation to Ta through O bridge.

concentration of dissolved O_2 in solution (1.26×10^{-3} mol L^{-1}).[13] As shown in Figure 11, the Koutecký–Levich plots of i_l^{-1} versus $\omega^{-1/2}$ at various potentials for the voltammograms of Figure 10a gave the straight lines the slopes of that are actually equal to that expected for four-electron ORR, and the values of n were found to be actually constant (4.0) in the examined range of potential (0.30 to 0.85 V) for the Pt/TaO_x/GC electrocatalyst. The n values were calculated to be 3.93 to 3.86 at E = 0.75 to 0.30 V for the Pt/GC electrocatalyst (Figure 10b).

3.4. Enhanced Oxygen Reduction Reaction. A spillover of, in particular oxygen-containing species is considered to be a dominant factor for the ORR enhancement at the Pt/TaO_x/GC electrocatalyst resulting from an electronic interaction between Pt and TaO_x. It should be noted that the electron in the d orbital is compulsory to form an electronic interaction between the Pt and the oxides.[7] Ta_2O_5 has no electron in the d orbital to be shared with the Pt, assuming that Pt was deposited on the Ta_2O_5 layer, as evidently proven from the XPS spectra (Figure 7). Therefore, as postulated previously in Section 3.2, the Pt may interact with O atom in Ta_2O_5 where the d orbital electron in Pt could be donated to Ta via O atoms, that is, through the bridging Ta–O–Pt bond resulting in the positive shift of Pt 4f spectra (Figure 6) and the lower binding energy peaks of Ta 4f spectra (Figure 7c). The formation of Ta–O–Pt bonds is similar to that of bridging Ta–O–support bonds proposed by Chen et al.[46] for supported tantalum oxide catalysts. The so-called oxygen spillover is well-known for a Pt/TiO_2 catalyst,[23,30,31] which has proven to possess a high ORR activity. In summary, it can be mentioned that (i) OH adsorbed on the Pt surface is spilled over to the TaO_x and (ii) the d orbital electron in Pt is donated to Ta through the bridging Ta–O–Pt bond, both of which facilitate the O_2 adsorption on the Pt surface, that is, the first step of the ORR, and finally result in the improved ORR (Figure 12). Here it should be mentioned that O_2 adsorption is facilitated as a result of the promoted vacant d orbital electron donation from Pt to Ta via the bridging Ta–O–Pt bond.[17] As can be seen in Figure 8, the remarkably enhanced intensity of peak currents, corresponding to the hydrogen adsorption–desorption and the Pt oxide layer formation and its reduction, at the Pt/TaO_x/GC electrocatalyst strongly suggests that a spillover phenomenon takes place during these surface redox reactions where the adsorbed species on the Pt could be spilled over to and back-spilled over from the TaO_x. Jaksic et al.[27,30] illustrated the spillover of primary oxide (M–OH) in TiO_2 and WO_3 as a continuous undisturbed reversible membrane mechanism where the OH is transferred by the altervalent change of M^{x+} and M^{x+1}. Moreover, they also considered that water molecules trapped inside the oxide introduce a water-oxide membrane composite that is important in the reversible reaction. Similarly, we presume that the species of Ta^{5+} and Ta^{m+} ($5 > m > 0$) as well as water molecules trapped in the oxides play the important roles in the spillover and back-spillover mechanisms in the Pt/TaO_x/GC electrocatalyst. In addition, this could also explain the negative impact of heat treatment on the spillover phenomenon at the Pt/TaO_x/GC electrocatalyst as being ascribed to the water loss. Further investigation is necessary to confirm the mechanism of enhanced ORR activity to optimize the activity of ORR on the Pt/TaO_x/GC electrocatalyst and to gain information on its long-term stability for PEMFC application.

4. CONCLUSIONS

In the present study, we have successfully fabricated a novel electrocatalyst of Pt/TaO_x/GC for ORR. A potential cycling technique for TaO_x electrodeposition was simply introduced to obtain nanosized particles of TaO_x on the GC surface. A homogenously dispersed TaO_x layer was produced; then, Pt nanoparticles were further electrodeposited on the TaO_x particles. For the Pt/TaO_x/GC electrocatalyst, we observed an interesting phenomenon of the so-called spillover effect. This effect was suspected to be due to the preferential adsorption of adsorbed H- and O-containing species onto the oxide and to result in a remarkable increase in the "apparent" surface area of Pt on the electrocatalyst. We also hypothesized that TaO_x has a crucial role in creating more active Pt sites for O_2 adsorption due to promoted vacancy of d orbital of Pt resulting from the electronic interaction between Pt and TaO_x. This consideration was evidently supported by the deconvolated XPS spectra. Therefore, both of these are considered to enhance the kinetics of O_2 reduction.

AUTHOR INFORMATION

Corresponding Author

*E-mail: ohsaka@echem.titech.ac.jp. Fax: +81-45-924-5489. Tel: +81-45-924-5404.

ACKNOWLEDGMENT

The present work was financially supported by Grant-in-Aid for Scientific Research (A) (no. 19206079) to T.O. from the Ministry of Education, Culture, Sport, Science and Technology (MEXT), Japan. Z.A. and J.M. gratefully acknowledge the Government of Japan for MEXT Scholarship.

REFERENCES

(1) Gasteiger, H. A.; Kocha, S. S.; Somaplli, B.; Wagner, F. T. *Appl. Catal., B* **2005**, *56*, 9–35.

(2) Watanabe, M.; Uchida, H. Electrocatalysis at Platinum and Bimetallic Alloys. In *Fuel Cell Catalysis: A Surface Science Approach*; Koper, M. T. M., Ed.; John Wiley & Sons, Inc.: Hoboken, NJ, 2009; pp 317−341.

(3) Gasteiger, H. A.; Markovic, N. M. *Science* **2009**, *324*, 48–49.

(4) Stamenkovic, V. R.; Mun., B. S.; Arenz, M.; Mayrhofer, K. J. J.; Lucas, C. A.; Wang, G.; Ross, P. N.; Markovic, N. M. *Nat. Mater.* **2007**, *6*, 241–247.

(5) Zhou, W. P.; Yang, X. F.; Vukmorovic, M. B.; Koel, B. E.; Jiao, J.; Peng, G.; Mavrikakis, M.; Adzic, R. R. *J. Am. Chem. Soc.* **2009**, *131*, 12755–12762.

(6) Murthi, V. S.; Urian, R. C.; Mukerjee, S. *J. Phys. Chem. B* **2004**, *108*, 11011–11023.

(7) Sasaki, K; Zhang, L.; Adzic, R. R. *Phys. Chem. Chem. Phys.* **2008**, *10*, 159–167.

(8) Selvaganesh, S. V.; Selvarani, G.; Sridhar, P.; Pitchumani, S.; Shukla, A. K. *J. Electrochem. Soc.* **2010**, *157*, B1000–B1007.

(9) Wilson, M. S.; Garzon, F. H.; Sickafus, K. E.; Gottesfeld, S. *J. Electrochem. Soc.* **1993**, *140*, 2872–2877.

(10) Stevens, D. A.; Dahn, J. R. *Carbon* **2005**, *43*, 179–188.

(11) Toda, T.; Igarashi, H; Uchida, H; Watanabe, M. *J. Electrochem. Soc.* **1999**, *146*, 3750–3756.

(12) Paulus, U. A.; Wokaun, A.; Scherer, G. G.; Schmidt, T. J.; Stamenkovic, V.; Radmilovic, V.; Markovic, N. M.; Ross, P. N. *J. Phys. Chem. B* **2002**, *106*, 4181–4191.

(13) Stamenkovic, V.; Schmidt, T. J.; Ross, P. N.; Markovic, N. M. *J. Phys. Chem. B* **2002**, *106*, 11970–11979.

(14) Jalan, V.; Taylor, E. J. *J. Electrochem. Soc.* **1983**, *130*, 2299–2302.

(15) Mukerjee, S.; Srinivasan, S. *J. Electroanal. Chem.* **1993**, *357*, 291–224.

(16) Mukerjee, S.; Srinivasan, S.; Soriaga, M. P. *J. Electrochem. Soc.* **1995**, *142*, 1409–1422.

(17) Toda, T.; Igarashi, H.; Watanabe, M. *J. Electrochem. Soc.* **1998**, *145*, 4185–4188.

(18) Hoshi, Y.; Yoshida, T.; Nishikata, A.; Tsuru, T. *Electrochim. Acta* **2011**, *56*, 5302–5309.

(19) Tauster, S. J.; Fung, S. C.; Baker, R. T. K.; Horsley, J. A. *Science* **1981**, *211*, 1121–1125.

(20) Ramaker, D. E.; de Graaf, J.; Veen, J. A. R. V.; Koningsberger, D. C. *J. Catal.* **2001**, *203*, 7–17.

(21) Conner, W. C., Jr.; Falconer, J. L. *Chem. Rev.* **1995**, *95*, 759–788.

(22) Kulesza, P. J.; Faulkner, L. R. *J. Electroanal. Chem.* **1989**, *259*, 81–98.

(23) Neophytides, S. G.; Murase, K.; Zafeiratos, S.; Papakonstantinou, G.; Paloukis, F. E.; Krstajic, N. V.; Jaksic, M. M. *J. Phys. Chem. C* **2006**, *110*, 3030–3042.

(24) Kohn, H. W.; Boudart, M. *Science* **1964**, *145*, 149.

(25) Benson, J. E; Kohn, H. W.; Boudart, M. *J. Catal.* **1966**, *5*, 307–313.

(26) Boudart, M.; Vannice, M. A.; Benson, J. E. *Z. Phys. Chem.* **1969**, *64*, 1–4.

(27) Jaksic, J. M.; Labou, D.; Papakonstantinou, G. D.; Siokou, A.; Jaksic, M. M. *J. Phys. Chem. C* **2010**, *114*, 18298–18312.

(28) Sermon, P. A.; Bond, G. C. *J. Chem. Soc., Faraday Trans. 1* **1980**, *76*, 889–900.

(29) Abbaro, S. A.; Tseung, A. C. C.; Hibbert, D. B. *J. Electrochem. Soc.* **1980**, *127*, 1106–1107.

(30) Jaksic, J. M.; Krstajic, N. V.; Vracar, L. M.; Neophytides, S. G.; Labou, D.; Falaras, P.; Jaksic, M. M. *Electrochim. Acta* **2007**, *53*, 349–361.

(31) Vracar, L. M.; Krstajic, N. V; Radmilovic, V. R.; Jaksic, M. M. *J. Electroanal. Chem.* **2006**, *587*, 99–107.

(32) Elezovic, N. R.; Babic, B. M.; Radmilovic, V. R.; Gojkoric, S. L.; Krstajic, N. V.; Vracar, L. M. *J. Power Sources* **2008**, *175*, 250–255.

(33) Elezovic, N. R.; Babic, B. M.; Radmilovic., V. R; Vracar, L. M.; Krstajic, N. V. *Electrochim. Acta* **2009**, *54*, 2404–2409.

(34) Bockris, J. O'M.; McHardy, J. *J. Electrochem. Soc.* **1973**, *120*, 61–66 .

(35) Shim, J.; Lee, C. R.; Lee, H. K.; Lee, J. S.; Cairns, E. J. *J. Power Sources* **2001**, *102*, 172–177.

(36) Vellacheri, R.; Unni, S. M.; Nahire, S.; Kharul, U. K.; Kurungot, S. *Electrochim. Acta* **2010**, *55*, 2878–2887.

(37) Shanmugram, S.; Gedanken, A. *J. Phys. Chem. C* **2009**, *113*, 18707–18712.

(38) Ioroi, T.; Siroma, Z.; Fujiwara, N.; Yamazaki, S.; Yasuda, K. *Electrochem. Commun.* **2005**, *7*, 183–188.

(39) Trogadas, P.; Ramani, V. *J. Electrochem. Soc.* **2008**, *155*, B696–B703.

(40) Tian, J.; Sun, G.; Cai, M.; Mao, Q.; Xin., Q. *J. Electrochem. Soc.* **2008**, *155*, B187–B193.

(41) Chhina, H.; Campbell, S.; Kesler, O. *J. Electrochem. Soc.* **2007**, *154*, B533–B539.

(42) Bauer, A.; Lee, K.; Song, C.; Xie, Y.; Zhang, J.; Hui, R. *J. Power Sources* **2010**, *195*, 3105–3110.

(43) Bonakdarpour, A.; Lobel, R.; Sheng, S.; Monchesky, T. L.; Dahn, J. R. *J. Electrochem. Soc.* **2006**, *153*, A2304–A2313.

(44) Borisenko, N.; Ispas, A.; Zschippang, E.; Liu, Q.; El Abedin, S. Z; Bund, A.; Endres, F. *Electrochim. Acta* **2009**, *54*, 1519–1528.

(45) Massot, L.; Chamelot, P.; Palau, P.; Taxil, P. *Electrochim. Acta* **2005**, *50*, 5408–5413.

(46) Chen, Y.; Fierro, J. L. G.; Tanaka, T.; Wachs, I. E. *J. Phys. Chem. B* **2003**, *107*, 5243–5250.

(47) Chen., Y.; Wachs, I. E. *J. Catal.* **2003**, *217*, 468–477.

(48) Ushikubo, T.; Wada, K. *App. Catal.* **1990**, *67*, 25–38.

(49) Macagno, V. A.; Schultze, J. W. *J. Electroanal. Chem.* **1984**, *180*, 157–170.

(50) Schultze, J. W.; Macagno, V. A. *Electrochim. Acta* **1986**, *31*, 355–363.

(51) Baturina, O. A.; Garsany, Y.; Zega, T. J.; Stroud, R. M.; Schull, T.; Swider-Lyons, K. E. *J. Electrochem. Soc.* **2008**, *155*, B1314–B1321.

(52) Wesselmark, M.; Wickman, B.; Lagergren, C.; Lindbergh, G. *Electrochim. Acta* **2010**, *55*, 7590–7596.

(53) Ferdousi, B. N.; Islam, M. M.; Okajima, T.; Mao., L.; Ohsaka, T. *Chem. Commun.* **2010**, *46*, 1165–1167.

(54) Kim, K. T.; Chung, J. S.; Lee, K. H.; Kim, Y. G. *Carbon* **1992**, *30*, 467–475.

(55) Antolini, E. *J. Mater. Sci.* **2003**, *38*, 2995–3005.

(56) Abdullah, A. M.; Saleh, M. M.; Awad, M. I.; Okajima; Kitamura, F.; Ohsaka, T. *J. Solid State Electrochem.* **2010**, *14*, 1727–1734.

(57) Khanuja, M.; Sharma, H.; Mehta, B. R.; Shivaprasad, S. M. *J. Electron Spectrosc. Relat. Phenom.* **2009**, *169*, 41–45.

(58) Takahagi, T.; Ishitani, A. *Carbon* **1988**, *26*, 389–396.

(59) Trasatti, S.; Petrii, O. A. *Pure Appl. Chem.* **1991**, *63*, 711–734.

(60) Garsany, Y; Baturina, O. A.; Swider−Lyons, K. E.; Kocha, S. S. *Anal. Chem.* **2010**, *82*, 6321–6328.

(61) Sata, S.; Awad, M. I.; El-Deab, M. S.; Okajima, T.; Ohsaka, T. *Electrochim. Acta* **2010**, *55*, 3528–3536.

(62) Masud, J.; Alam, M. T.; Miah, M. R.; Okajima, T.; Ohsaka, T. *Electrochem. Commun.* **2011**, *13*, 86–89.

(63) Hillenbrand, L. J.; Lacksonen, J. W. *J. Electrochem. Soc.* **1965**, *112*, 249–252.

(64) Shukla, A. K.; Ravikumar, M. K.; Roy, A; Barman, S. R.; Sarma, D. D.; Arico, A. S.; Antonucci, V.; Dino., L.; Giordano, N. *J. Electrochem. Soc.* **1994**, *141*, 1517–1522.

(65) Takasu, Y.; Ohashi, N.; Zhang, X. G.; Murakami, Y.; Minagawa, H.; Sato, S.; Yahikozawa, K. *Electrochim. Acta* **1996**, *41*, 2595.

(66) Marcus, P.; Hinnen, C. *Surf. Sci.* **1997**, *392*, 134–142.

(67) Escard, J.; Leclere, C.; Contour, J. P. *J. Catal.* **1973**, *29*, 31–39.

(68) Horsley, J. A. *J. Am. Chem. Soc.* **1979**, *101*, 2870–2874.

(69) Savadogo, O.; Beck, P. J. *J. Electrochem. Soc.* **1996**, *143*, 3842–3846.

(70) Paulus, U. A.; Schmidt, T. J.; Gasteiger, H. A.; Behm, R. J. *J. Electroanal. Chem.* **2001**, *495*, 134–145.
(71) Damjanovic, A.; Brusic, V. *Electrochim. Acta* **1967**, *12*, 615–628.
(72) Sepa, D. B.; Vojnovic, M. V.; Damjanovic, A. *Electrochim. Acta* **1981**, *26*, 781.
(73) Wang, J. X.; Uribe, F. A.; Springer, T. E.; Zhang, J.; Adzic, R. R. *Faraday Discuss.* **2008**, *140*, 347–362.